

Element-specific analysis of the magnetic anisotropy in Mn-based antiferromagnetic alloys from first principles

S. Khmelevskyi,^{1,2} A. B. Shick,² and P. Mohn¹

¹Center for Computational Materials Science, Institute of Applied Physics, Vienna University of Technology, Gusshausstrasse 25a, AT-1040 Vienna, Austria

²Institute of Physics ASCR, v.v.i., Na Slovance 2, CZ-182 21 Praha 8, Czech Republic

(Received 3 August 2010; published 27 June 2011)

The magnetic anisotropy energy (MAE) and element-specific contributions to the MAE have been studied for Mn-based antiferromagnetic alloys with layered L₁₀ structure within the framework of the local spin-density approximation and the fully relativistic torque method. It is found that the contribution to the total MAE from nonmagnetic 3d and 4d elements in MnNi and MnPd alloys are comparable to the contribution of the magnetic Mn atoms. In the 3d-5d MnIr and the 4d-5d MnRh alloys the Ir and Rh contributions are found to be dominating. The origin of this nonzero contribution into the MAE from the atom with zero spin moment is linked to the nontrivial atomic spin density distribution, which gives a zero moment only on average. We also find and discuss the strong dependence of the total and element-specific contributions to the MAE on the state of magnetic order.

DOI: 10.1103/PhysRevB.83.224419

PACS number(s): 75.45.+j, 75.50.Ee, 75.30.Gw

I. INTRODUCTION

Magnetic anisotropy is a fundamental property of magnetically ordered materials and is responsible for a variety of macroscopically observed and technologically important effects. On a microscopical level magnetic anisotropy originates from the relativistic spin-orbit coupling (SOC), which is much weaker than the electrostatic Coulomb and exchange interaction. This allows us to treat anisotropy in magnetic solids using perturbation theory. In the case of rare-earth magnetism, where the magnetic moments are well localized and spin-orbit interaction is stronger than the effects of the crystal field, the perturbation theory approach leads to a comprehensible microscopic description of the magnetic anisotropy effects.¹ In transition metal systems where the magnitude of the magnetic anisotropy is much smaller (due to the quenching of the orbital moments by the crystal field) the magnetic anisotropy energy appears only at second and higher orders of the perturbation expansion over the SOC.²

First-principles calculations of the magnetic anisotropy energy within a relativistic band theory based on the local spin-density approximation (LSDA) for elemental cubic ferromagnetic transition metals such as Fe and Ni were only partially successful.³ This so-called cubic magnetic anisotropy energy (MAE) occurs in the fourth-order SOC perturbation series, and extremely small values of this MAE (a few $\mu\text{eV}/\text{atom}$) are beyond the accuracy of LSDA. In fact, the calculations of the cubic MAE in especially Ni experience severe difficulties even with computational stability, e.g., k -point convergence, etc. (see, e.g., Ref. 3 and the discussion given in Ref. 4). Even in the case of elemental hcp Co, with a uniaxial MAE of the order of a few tens of $\mu\text{eV}/\text{atom}$, which corresponds to the second-order SOC perturbation, LSDA results are controversial.⁵

Nevertheless, relativistic band structure calculations can well describe the MAE in *d*-transition-metal-based ferromagnetic multilayers,^{6–8} surfaces and overlayers,⁹ low-dimensional nanostructures,¹⁰ and ad-atoms on surfaces,¹¹ where the values of MAE are sometimes two to three orders of magnitude larger than in elemental 3d metals. Technologically important systems that have recently attracted considerable theoretical interest are ordered FePt^{12,13} and CoPt ferromag-

netic (FM) alloys with L₁₀ structure. It appears that alloying of a nonmagnetic 5d element to Fe or Co leads to a strong (almost two orders of magnitude) enhancement of the magnetic anisotropy energy as compared to elemental Co, which has been very well captured by first-principles calculations using various methods.^{14–16} The proposed explanation of this enhancement is a sizable spin-orbit coupling on 5d Pt atoms, which strongly contributes to the MAE due to the spin polarization of the Pt atoms by the magnetic 3d metals. In this scenario the contribution to MAE from Pt can be expressed as the product of the square of the SOC and the square of the induced magnetic moment on Pt. We note that this mechanism is beyond the reach of the existing analytical model attempts to analyze magnetic anisotropy effects in transition metals, for example, in Bruno's model,¹⁷ and its extension⁴ relied on coupling between SOC and the local magnetic moment at the same atomic site.

By putting together the above-mentioned arguments the large value of the magnetic anisotropy (≈ 3.5 meV/f.u.) in the antiferromagnetic (AFM) alloy MnIr with L₁₀ structure found in earlier calculations^{18,19} is quite noticeable. This value appears to be more than twice that in the ferromagnetic alloy FePt. Other Mn-based AFMs with L₁₀ structure, namely MnX (X = Pt, Ni, Rh, Pd), were also shown to exhibit a large-magnitude MAE (≈ 0.1 –1 meV),¹⁸ although not as strong as in MnIr. It should be mentioned that due to the symmetry of the AFM ground state, which leads to a compensation of the exchange fields of the surrounding Mn atoms, the X sites have no induced magnetic moment. In order to clarify the mechanism of the MAE enhancement in these AFM alloys we have revisited the first-principle study of these systems, choosing as alloying element 3d Ni, 4d Pd, and 5d Ir. In addition to the previous studies we perform an element-specific analysis of the contributions to the MAE in MnX from different atomic species (Mn, X = Ni, Pd, Ir) using the torque method. What we find is that despite a total zero atomic moment on the X sites the contribution to the MAE from the nonmagnetic element is essential. Even in the case of MnNi the Ni contribution is of the same order of magnitude as from magnetic Mn, whereas in MnIr the Ir contribution dominates. We also study the MAE in these systems in the FM

state. This allows us to draw some nontrivial conclusions by making a comparison with the AFM ground state.

In general, it is much more difficult to measure experimentally the MAE in compensated AFM materials with zero net magnetization, which makes it rigid to the external magnetic field. Until recently, the MAE of AFMs was studied experimentally much less than in FM materials, probably due to limited technological interest. From a practical point of view, current interest to the MAE in the AFM MnX (X = Ni, Pd, Ir) alloys originates from their applicability as pinning layers in exchange bias systems. There exists a whole class of so-called practical AFM alloys²⁰ where the anisotropy of the bulk AFM substrate plays a leading role in many theories of the exchange bias.²¹ Moreover, recent experiments²² suggest unambiguously that the exchange bias effect is strongly governed by the bulk properties of the AFM substrate. In addition we would like to mention a recently proposed idea to use the huge anisotropy of AFMs, in particular with L1₀ structure, for applications in spintronics utilizing the associated huge anisotropic tunneling magnetoresistance effect.²³

II. COMPUTATIONAL METHOD AND DETAILS

We employ the relativistic version of the full-potential linear augmented plane-wave (FP-LAPW) method.²⁴ The SOC is included in a self-consistent second-variational procedure.²⁵ The exchange and correlation effects are treated within the framework of the local spin-density approximation using the parametrization by von Barth and Hedin,²⁶ which is expected to be valid for itinerant metallic systems. All calculations are done for the experimental lattice structure. The lattice parameters of the tetragonal L1₀ structure (Fig. 1) are taken to be $a = 7.035$ a.u., $c/a = 0.945$ for MnNi; $a = 7.689$ a.u., $c/a = 0.882$ for MnPd; and $a = 7.281$ a.u., $c/a = 0.945$ for MnIr.^{20,27,28}

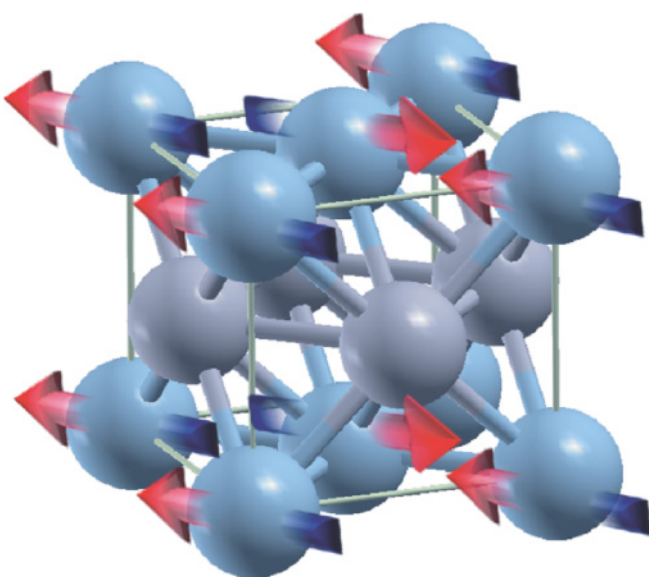


FIG. 1. (Color online) L1₀ structure of MnX and magnetic ordering in the AFM ground state. Blue balls (arrows show the mutual spin orientation) are Mn-atoms, grey balls (without arrows) are Ni, Pd, and Ir, respectively.

At first, the self-consistent charge and spin densities were calculated for the magnetic moment aligned along the [001] z axis using the Brillouin zone (BZ) sampling with 1000 k points. Next, the MAE was evaluated using the torque method.^{29,30} It can be formulated as follows. We solve the Kohn-Sham equations for a two-component spinor $|\Phi_i\rangle = (\Phi_i^\uparrow, \Phi_i^\downarrow)$,

$$\sum_\beta (-\nabla^2 + \hat{V}_{\text{eff}} + \xi(\vec{l} \cdot \vec{s}))_{\alpha,\beta} \Phi_i^\beta(\mathbf{r}) = e_i \Phi_i^\alpha(\mathbf{r}), \quad (1)$$

where the $\hat{V}_{\text{eff}} = V(\mathbf{r})\hat{I} + \boldsymbol{\sigma} \cdot \mathbf{B}(\mathbf{r})$ matrix consists of the sum of the scalar potential V and the “exchange” field B parallel to the spin moment M_S , and $\hat{H}_{\text{SO}} = \xi(\vec{l} \cdot \vec{s})$ is the SOC operator. Here, to simplify the notation, we use a Pauli-like Hamiltonian including spin-orbit coupling, while the actual implementation contains in addition the scalar-relativistic terms.³¹ When the magnetic force theorem is used to evaluate the magnetocrystalline anisotropy energy, M_S is rotated and a single energy band calculation is performed for the new orientation of M_S . The MAE results from SO coupling induced changes in the band eigenvalues

$$E_A(\theta, \phi) = \sum_i^{occ} \epsilon_i(\theta, \phi). \quad (2)$$

Alternatively, the torque $T(\theta, \phi) = \partial E_A(\theta, \phi)/\partial\theta$ can be evaluated within the linear response theorem and reads

$$T(\theta, \phi) = \sum_i^{occ} \langle \Phi'_i | \frac{\partial \mathbf{U}}{\partial \theta} \xi(\vec{l} \cdot \vec{s}) \mathbf{U}^\dagger + \mathbf{U} \xi(\vec{l} \cdot \vec{s}) \frac{\partial \mathbf{U}^\dagger}{\partial \theta} | \Phi'_i \rangle, \quad (3)$$

where $\mathbf{U}(\theta, \phi)$ is a conventional spin rotation matrix and $|\Phi'\rangle = \mathbf{U}(\theta, \phi)|\Phi\rangle$.

The LAPW basis function $\phi_{\mathbf{k}+\mathbf{G}}^\sigma(\mathbf{r})$ is a plane wave $\exp(i(\mathbf{k}+\mathbf{G}) \cdot \mathbf{r})$ outside of the muffin tin sphere, inside α ($\mathbf{r}_i = \mathbf{r} - \mathbf{R}_\alpha$) it is a linear combination of the radial functions:

$$\phi_{\mathbf{k}+\mathbf{G}}^\sigma(\mathbf{r}) = \sum_{l,m} [a_{\mathbf{k}+\mathbf{G}}^{lm} u_l^\sigma(r_i) + b_{\mathbf{k}+\mathbf{G}}^{lm} \dot{u}_l^\sigma(r_i)] Y_{lm}(\hat{r}_i), \quad (4)$$

where u_l , \dot{u}_l are the radial wave function and its energy derivative at an appropriate energy E_l for angular quantum number l (recall that $\langle u_l | u_l \rangle = 1$, $\langle u_l | \dot{u}_l \rangle = 0$), \mathbf{k} is a k point in BZ, and \mathbf{G} is any reciprocal lattice vector.

The solution of the Kohn-Sham equations $|\Phi'\rangle = \mathbf{U}(\theta, \phi)|\Phi\rangle$ is

$$\begin{aligned} \Phi_k'^{b,\uparrow}(\mathbf{r}) &= \sum_{\mathbf{G}} c_{\mathbf{k}+\mathbf{G}}^{b,\uparrow} \phi_{\mathbf{k}+\mathbf{G}}^\uparrow(\mathbf{r}), \\ \Phi_k'^{b,\downarrow}(\mathbf{r}) &= \sum_{\mathbf{G}} c_{\mathbf{k}+\mathbf{G}}^{b,\downarrow} \phi_{\mathbf{k}+\mathbf{G}}^\downarrow(\mathbf{r}), \end{aligned} \quad (5)$$

where b is the band index and the sum runs over reciprocal lattice vectors. The torque equation (3) reads

$$\begin{aligned} T(\theta, \phi) &= \sum_{\alpha} \sum_{\mathbf{k}, b} w(\mathbf{k}, b) \sum_{l, m_l, m'_l} \sum_{s, s'} \sum_{\mathbf{G}, \mathbf{G}'} c_{\mathbf{k}+\mathbf{G}}^{*b,s} c_{\mathbf{k}+\mathbf{G}'}^{b,s'} \\ &\times \langle l, m_l, s | \frac{\partial \mathbf{U}}{\partial \theta} (\vec{l} \cdot \vec{s}) \mathbf{U}^\dagger + \mathbf{U} (\vec{l} \cdot \vec{s}) \frac{\partial \mathbf{U}^\dagger}{\partial \theta} | l, m'_l, s' \rangle \\ &\times (a_{\mathbf{k}+\mathbf{G}}^{*\alpha, l, m, s} a_{\mathbf{k}+\mathbf{G}'}^{\alpha, l, m', s'} \xi_{l, s, s'}^\alpha + a_{\mathbf{k}+\mathbf{G}}^{*\alpha, l, m, s} b_{\mathbf{k}+\mathbf{G}'}^{\alpha, l, m', s'} \dot{\xi}_{l, s, s'}^\alpha \\ &+ b_{\mathbf{k}+\mathbf{G}}^{*\alpha, l, m, s} a_{\mathbf{k}+\mathbf{G}'}^{\alpha, l, m', s'} \dot{\xi}_{l, s', s}^\alpha + b_{\mathbf{k}+\mathbf{G}}^{*\alpha, l, m, s} b_{\mathbf{k}+\mathbf{G}'}^{\alpha, l, m', s'} \ddot{\xi}_{l, s', s}^\alpha), \end{aligned} \quad (6)$$

where $w(\mathbf{k}, b)$ is the weight of band b for the k point \mathbf{k} ,

$$\begin{aligned}\xi_{l,s,s'}^{\alpha} &= \int_0^{R_a} dr r \frac{1}{2(Mc)^2} \frac{dV(r)}{dr} u_{l,s}(r) u_{l,s'}(r), \\ \dot{\xi}_{l,s,s'}^{\alpha} &= \int_0^{R_a} dr r \frac{1}{2(Mc)^2} \frac{dV(r)}{dr} \dot{u}_{l,s}(r) u_{l,s'}(r), \\ \ddot{\xi}_{l,s,s'}^{\alpha} &= \int_0^{R_a} dr r \frac{1}{2(Mc)^2} \frac{dV(r)}{dr} \dot{u}_{l,s}(r) \dot{u}_{l,s'}(r),\end{aligned}\quad (7)$$

and $M = m + [E_l - V(r)]/2c^2$ is the so-called relativistic mass.

The torque equation (6) then has been calculated at different spherical angles using 5324 k points in the BZ to ensure convergence of the torque and MAE values to better than 0.01 meV/f.u. Thus the torque method²⁹ allows us to make a separation of the contributions in Eq. (6) into torques arising from the spin-orbit coupling on different atomic sites α in the unit cell.³⁰

III. RESULTS AND DISCUSSION

For a tetragonal L1₀ structure the crystal symmetry of the MAE can be expressed as a function of the spherical angles θ and ϕ as³²

$$E(\theta, \phi) = K_{2\perp} \sin^2 \theta + K_{4\perp} \sin^4 \theta + K_{4\parallel} \sin^4 \theta \cos 4\phi. \quad (8)$$

Here $K_{2\perp}$ is the uniaxial MAE constant, and $K_{4\perp}$ and $K_{4\parallel}$ are the fourth-order out-of-plane and in-plane MAE constants, respectively (with the z axis of a spherical coordinate system being along the tetragonal c direction). Then the torque becomes

$$T(\theta, \phi) = K_{2\perp} \sin 2\theta + 2[K_{4\perp} + K_{4\parallel} \cos 4\phi] \sin^2 \theta \sin 2\theta. \quad (9)$$

The dependence of the torque on the polar angle ϕ in the present alloys is found to be very small (much less than 0.01 meV/f.u., i.e., few orders of magnitude smaller than the θ dependence). Thus we will ignore this dependence in the following discussion.

In Fig. 2 the results of our calculations for the θ dependence of the total torque and the atom-resolved contributions in the AFM state (see Fig. 1) are presented for MnNi, MnPd, and MnIr. The AFM state has the lowest energy, in agreement with experiment.²⁰ The calculations were performed by keeping the angle ϕ fixed at $\pi/8$, and the resulting values were fitted according to Eq. (9). Note that the value of the torque for $\theta = \pi/4$ gives the value of the magnetic anisotropy energy (Fig. 2). In all cases considered the value of the total torque and the MAE are negative, yielding the easy-plane anisotropy in MnNi, MnPd, and MnIr.

The magnetic moments in the AFM state on Ni, Pd, and Ir are found to be zero, as is expected for the compensated AFM. Nevertheless, as can be seen from Fig. 2, these atoms provide the essential contribution to the total torque and magnetic anisotropy. In the 3d-5d alloy (MnIr) the Ir contribution is dominating and in the 3d-4d alloy (MnPd) the Pd contribution is almost the same as the contribution from Mn with a magnetic moment of 3.67 μ_B /atom. Even 3d Ni with zero magnetic moment provides almost half of the the total torque and MAE for MnNi. From the point of view of the model theories^{4,17}

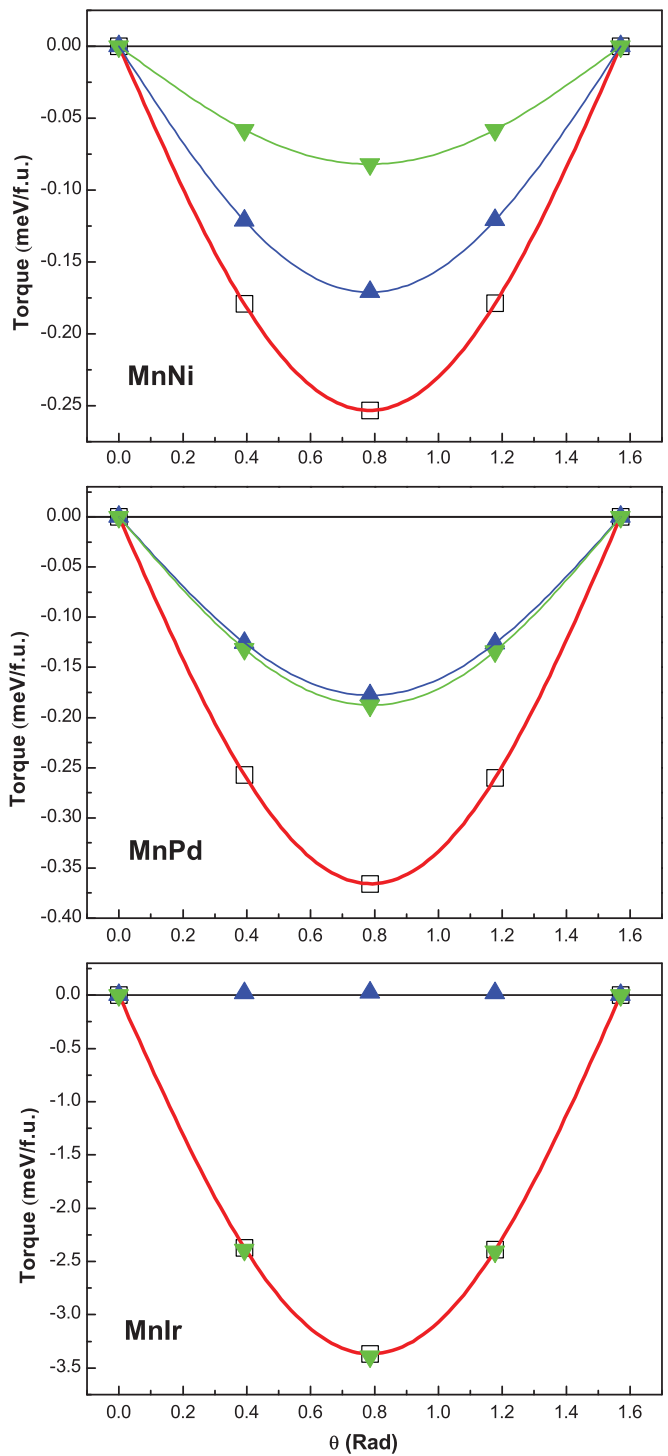


FIG. 2. (Color online) Total (red lines, open squares) and atom-resolved contribution to the torque; the Mn part is given by the blue lines (up triangles) and the X atom part is given in green (down triangles).

of the magnetic anisotropy in itinerant FMs, which operate with total spin and total orbital atomic moment only, this result is somehow counterintuitive, since Ir, Pd, and Ni do not contribute to the total spin and orbital moment. Nevertheless, the spin-orbit interaction in these atoms strongly depends on the direction of the moments of the Mn matrix. This is

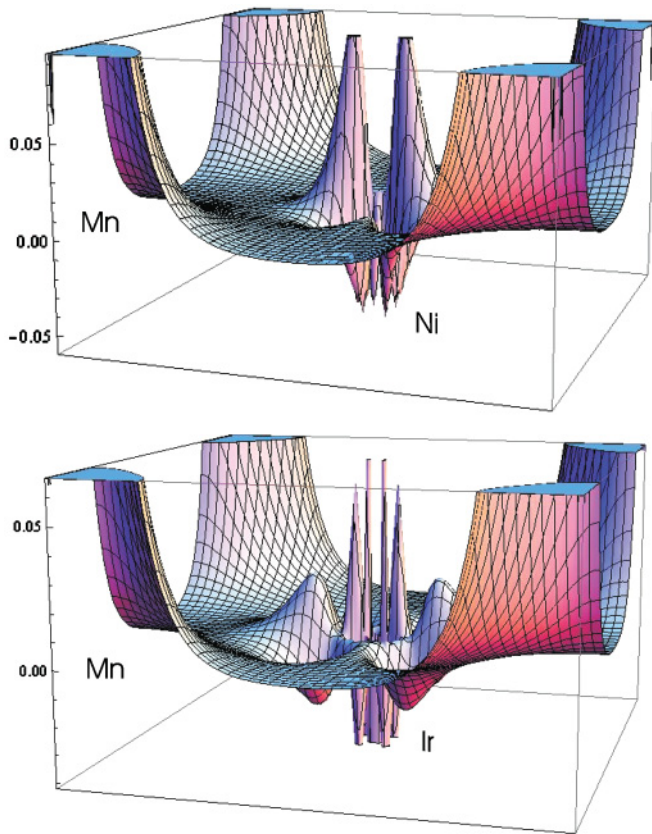


FIG. 3. (Color online) Spin density in the [100] plane for AFM MnNi and MnIr.

explained by the fact that Ni, Pd, and Ir show a local induced spin-polarization, which only provides a zero total moment after integration of the spin density over the respective atomic sphere.

In Fig. 3 we present the calculated spin density plots for MnNi and MnIr alloys in the [100] plane. The magnetic Mn atoms with large spin moment and correspondingly very high spin density and parallel moment are in the corners. The Ni and Ir atoms with total zero moments are in the center. The local spin polarization on Ni and Ir is quite large, but it is clearly seen that it has regions with positive and negative values. The dependence of this spin-density distribution on the orientation of the AFM staggered magnetization direction is responsible for the SOC energy angular dependence. This SOC energy dependence on the AFM staggered magnetization direction determines the contribution to the total torque and the MAE

from these sites with zero magnetization. The relative values of the Ir, Pd, and Ni atom contributions to MAE can be easily be understood from the fact that the spin-orbit coupling in the d shell is increasing with an increase in principal quantum number.

The calculated values of the magnetic moments on the Mn atom, the uniaxial anisotropy constants $K_{2\perp}$, and the MAE (total and element X = Ni, Pd, Rh, Ir resolved) for the AFM ground state are collected in Table I. One finds that the spin moment of Mn in MnIr is different from that in MnNi and MnPd but this difference does not immediately explain why the MAE for Mn in MnIr almost vanishes. The possible reason for this behavior is that the Mn moment in MnIr is an weak-itinerant (unsaturated) moment, while for both MnNi and MnPd the moments become localized. It is also interesting to note that the spin-orbit interaction on Mn sites in MnIr alloy tends to create an easy-axis anisotropy (positive sign of the respective contribution to the MAE), while the dominating Ir contribution leads to a strong easy-plane anisotropy. Our calculated total MAE for MnIr (-3.37 meV/f.u.) is in excellent agreement with earlier non-full-potential studies of MnIr (-3.53 meV/f.u.)¹⁸ and (-3.41 meV/f.u.).¹⁹ Our FP-LAPW results give somewhat larger values of the easy-plane MAE for MnNi (-0.25 meV/f.u.) and MnPd (-0.36 meV/f.u.) than given in the calculations by Umetsu *et al.*¹⁸ (-0.15 and -0.29 meV/f.u., respectively). By taking into account the smallness of the MAE values the agreement can be regarded as quite fair. Despite the fact that MnRh forms a highly disordered alloy²⁰ we add our results for a fully ordered compound for the sake of comparison with the isoelectronic MnIr. Since Rh is a $4d$ element we expect that the SOC is smaller than that for Ir. Indeed, as can be seen from Table I, the MAE in MnRh is almost one order of magnitude smaller than for MnIr. This result again shows that the MAE mainly comes from the SOC at the heavier element. Although the experimental determination of the MAE in the AFM alloys with L₁₀ structure is difficult (see discussion in Refs. 20 and 18), the successful description of the MAE in their ferromagnetic counterparts FePt and CoPt^{14,15} gives us confidence in the present results as well as in the results of earlier MAE studies for AFM alloys.

We now turn to the question of the dependence of the magnetic anisotropy energy on the state of the magnetic order. We have calculated the torque in the FM state where all Mn atoms have magnetic moments pointing in the same direction. The experimental lattice constants and c/a ratios are used as in the AFM calculations. The FM state is higher in energy

TABLE I. Magnetic moments on Mn (spin m_s and orbital m_l), magnetic anisotropy constants $K_{2\perp}$ and $K_{4\perp}$ [see Eq. (8)], magnetic anisotropy energy (MAE), and element-resolved contribution to MAE of MnX (X = Ni, Pd, Rh, Ir) alloys calculated for the AFM ground state.

MnX	m (μ_B/Mn)		$K_{2\perp}, K_{4\perp}$ (meV/f.u.)	MAE (meV/f.u.)		
	m_s	m_l		total	Mn	X
MnNi	3.12	0.02	$-0.25, 0.00$	-0.25	-0.17	-0.08
MnPd	3.67	0.01	$-0.36, 0.00$	-0.36	-0.18	-0.18
MnRh	3.00	0.02	$-0.43, 0.00$	-0.43	-0.01	-0.42
MnIr	2.64	0.05	$-3.35, -0.02$	-3.37	0.03	-3.40

TABLE II. Atomic magnetic moments on Mn and X sites (spin m_s and orbital m_l), magnetic anisotropy energy (MAE), and element-resolved contribution to MAE of MnX (X = Ni, Pd, Rh, Ir) alloys calculated for ferromagnetic state.

MnX	m(Mn) (μ_B)		m(X) (μ_B)		MAE (meV/f.u.)		
	m_s	m_l	m_s	m_l	total	Mn	X
MnNi	3.15	0.01	0.61	0.04	-0.01	-0.20	0.19
MnPd	3.74	0.01	0.34	-0.03	0.07	-0.08	0.15
MnRh	3.05	0.03	0.08	-0.01	-0.13	0.17	-0.30
MnIr	1.56	0.01	-0.11	-0.01	-0.24	0.26	-0.50

than the AFM ground state for all three alloys, in agreement with experiment. The Mn local-moments-induced exchange fields are no longer compensated on the Ni, Pd, and Ir sites. They have nonzero induced total spin and orbital moments (see Table II). We find that the moments on Ir are antiparallel to the direction of the Mn ferromagnetic matrix, whereas Ni and Pd are polarized parallel to the direction of the Mn magnetization. Compared to the AFM ground state, the values of the spin moments on Mn atoms in the FM state remain almost the same, suggesting that they are well localized. This is in contrast to MnIr, where Mn loses in value almost 1 μ_B /atom compared to the AFM state. Nevertheless, the changes of the element-resolved contributions to the MAE do not follow either the value of the total atomic moments or the values of the orbital moments. The Ni and Pd atom element-specific contributions to the MAE strongly depend on the type of long-range magnetic order (AFM or FM). These changes greatly affect the total MAE. On Ni and Pd the MAE changes from easy plane to easy axis when AFM is changed to FM. The Mn atom contributions always remain as easy-plane anisotropy.

In ferromagnetic MnNi, the contribution from Ni becomes comparable in size to that of Mn, leading to a vanishing total MAE. A similar but incomplete compensation occurs in MnPd. However, when compared to the AFM state, the Pd contribution becomes larger than the Mn contribution so that the total anisotropy changes to the easy axis. We note also that the calculated values of the total MAE in the FM state of MnNi and MnPd are in excellent agreement with Full Potential-Linear Muffin Tin Orbital (FP-LMTO) results by Ravindran *et al.*,³³ who restricted their calculations to the FM state only. For the FM state of MnIr, one finds that the Ir contribution surprisingly becomes much smaller than in the AFM state despite that in the FM state the Ir atoms

have a nonzero total spin-polarization and orbital moment. In contrast, the Mn contribution to the MAE increases by almost by one order of magnitude compared to the AFM state although the total spin and total orbital moment essentially decrease.

It thus appears that the element-specific contribution to the MAE essentially depends on the state of magnetic order. In this respect we note that one should be very careful in mapping results of a MAE calculation onto phenomenological spin Hamiltonians which include only single-site and two-site terms, since the contribution from the nonmagnetic element to the MAE depends on the orientation of all surrounding atomic moments. Such a strong dependence can lead to multisite anisotropic terms beyond the two-site ones usually included in phenomenological Hamiltonians.¹⁹

IV. CONCLUSIONS

We conclude that the large contributions to the MAE from the nonmagnetic elements in antiferromagnetic MnX (X = Ni, Pd, Ir) alloys with L₁₀ structure are due to nontrivial spin-polarization of these elements by the surrounding Mn atoms. Although the total spin and orbital moments are zero, there exists a strong dependence of the SOC on these sites on the direction of the staggered Mn magnetization. Interestingly, the 3d Ni atom provides a contribution to the MAE which is similar in size to those from Mn with well-localized intrinsic magnetic moments. In the case of MnIr the Ir contribution is dominant, resulting in a large total MAE, which together with high Neel temperature and consequently large exchange stiffness demands an application of this material in exchange bias technology. The element-specific and total MAE strongly depend on the magnetic order: the MAE changes from easy-plane to easy-axis anisotropy between the AFM and FM states. The element-specific contributions to the MAE from different atomic species show rather nontrivial and sometimes counterintuitive dependence on the total spin and orbital moment at a specific atomic site.

ACKNOWLEDGMENTS

S.K. acknowledges the support from the Austrian Ministry of Science and Research within the MOEL program managed by the Österreichische Forschungsgemeinschaft. Financial support from Czech Republic Grants No. GACR P204/10/0330, No. GAAV IAA100100912, and No. AV0Z10100520 is acknowledged.

¹J. Jensen and A. R. Mackintosh, *Rare Earth Magnetism* (Oxford, Clarendon, 1991).

²R. M. White, *Quantum Theory of Magnetism* (Springer-Verlag, Berlin, Heidelberg, New York, 1983).

³G. H. O. Daalderop, P. J. Kelly, and M. F. H. Schuurmans, *Phys. Rev. B* **41**, 11919 (1990).

⁴G. van der Laan, *J. Phys. Condens. Matter* **10**, 3239 (1998).

⁵M. D. Stiles, S. V. Halilov, R. A. Hyman, and A. Zangwill, *Phys. Rev. B* **64**, 104430 (2001).

⁶G. H. O. Daalderop, P. J. Kelly, and M. F. H. Schuurmans, *Phys. Rev. B* **44**, 12054 (1991).

⁷T. Burkert, L. Nordstrom, O. Eriksson, and O. Heinonen, *Phys. Rev. Lett.* **93**, 027203 (2004).

⁸G. Andersson, T. Burkert, P. Warnicke, M. Bjorck, B. Sanyal, C. Chacon, C. Zlotea, L. Nordstrom, P. Nordblad, and O. Eriksson, *Phys. Rev. Lett.* **96**, 037205 (2006).

⁹B. Ujfaluassy, L. Szunyogh, P. Bruno, and P. Weinberger, *Phys. Rev. Lett.* **77**, 1805 (1996).

- ¹⁰A. B. Shick, F. Maca, and P. M. Oppeneer, *Phys. Rev. B* **69**, 212410 (2004).
- ¹¹P. Blonski, A. Lehnert, S. Dennler, S. Rusponi, M. Etzkorn, G. Moulas, P. Bencok, P. Gambardella, H. Brune, and J. Hafner, *Phys. Rev. B* **81**, 104426 (2010).
- ¹²D. Weller and A. Moser, *Proc. IEEE Trans. Magn.* **36**, 10 (1999).
- ¹³O. N. Mryasov, U. Nowak, K. Y. Guslienko, and R. W. Chantrell, *Europhys. Lett.* **69**, 805 (2005).
- ¹⁴A. B. Shick and O. N. Mryasov, *Phys. Rev. B* **67**, 172407 (2003).
- ¹⁵I. Galanakis, M. Alouani, and H. Dreyssse, *Phys. Rev. B* **62**, 6475 (2000).
- ¹⁶J. B. Staunton, S. Ostanin, S. S. A. Razee, B. L. Gyorffy, L. Szunyogh, B. Ginatempo, and E. Bruno, *Phys. Rev. Lett.* **93**, 257204 (2004).
- ¹⁷P. Bruno, *Phys. Rev. B* **39**, 865 (1989).
- ¹⁸R. Y. Umetsu, A. Sakuma, and K. Fukamichi, *Appl. Phys. Lett.* **89**, 052504 (2006).
- ¹⁹L. Szunyogh, B. Lazarovits, L. Udvardi, J. Jackson, and U. Nowak, *Phys. Rev. B* **79**, 020403(R) (2009).
- ²⁰K. Fukamichi, R. Y. Umetsu, A. Sakuma, and C. Mitsumata, in *Handbook of Magnetism and Magnetic Materials*, edited by K. H. J. Buschow (Elsevier, Dordrecht, 2006), Vol. 16, p. 209.
- ²¹D. Mauri, H. C. Siegmann, P. S. Bagus, and E. Kay, *J. Appl. Phys.* **57**, 3047 (1987).
- ²²R. Morales, Z.-P. Li, J. Olamit, K. Liu, J. M. Alameda, and I. K. Schuller, *Phys. Rev. Lett.* **102**, 097201 (2009).
- ²³A. B. Shick, S. Khmelevskyi, O. N. Mryasov, J. Wunderlich, and T. Jungwirth, *Phys. Rev. B* **81**, 212409 (2010).
- ²⁴E. Wimmer, H. Krakauer, M. Weinert, and A. J. Freeman, *Phys. Rev. B* **24**, 864 (1981).
- ²⁵A. B. Shick, D. L. Novikov, and A. J. Freeman, *Phys. Rev. B* **56**, 14259 (1997).
- ²⁶U. von Barth and L. Hedin, *J. Phys. C* **5**, 1629 (1972).
- ²⁷K. H. J. Buschow, P. G. van Eugen, and R. R. Johngebret, *J. Magn. Magn. Mater.* **38**, 1 (1983).
- ²⁸K. Brun, A. Kjekshus, and W. B. Pearson, *Philos. Mag.* **10**, 291 (1964).
- ²⁹X. Wang, R. Wu, D.-S. Wang, and A. J. Freeman, *Phys. Rev. B* **54**, 61 (1996).
- ³⁰A. B. Shick, F. Maca, M. Ondracek, O. N. Mryasov, and T. Jungwirth, *Phys. Rev. B* **78**, 054413 (2008).
- ³¹A. H. MacDonald, W. E. Pickett, and D. D. Koelling, *J. Phys. C* **13**, 2675 (1980).
- ³²S. Chikazumi, *Physics of Ferromagnetism* (Oxford University Press, Oxford, 2009).
- ³³P. Ravindran, A. Kjekshus, H. Fjellvaag, P. James, L. Nordström, B. Johansson, and O. Eriksson, *Phys. Rev. B* **63**, 144409 (2001).